

Study of energy response and resolution of the ATLAS barrel calorimeter to hadrons of energies from 20 to 350 GeV

E. Abat^{a,1}, J.M. Abdallah^b, T.N. Addy^c, P. Adragna^d, M. Aharrouche^e, A. Ahmad^f, T.P.A. Akesson^g, M. Aleksa^h, C. Alexaⁱ, K. Anderson^j, F. Anghinolfi^h, A. Antonaki^k, G. Arabidze^k, E. Arik^a, O.K. Baker^l, D. Banfi^m, S. Baron^h, H.P. Beckⁿ, B. Belhorma^o, D. Benchekroun^p, D.P. Benjamin^q, K. Benslama^f, E. Bergeaas Kuutmann^s, H. Bertelsen^t, S. Binet^u, C. Biscarat^v, V. Boldeaⁱ, V.G. Bondarenko^w, M. Boonekamp^x, M. Bosman^b, C. Bourdarios^u, D. Burckhart Chromek^h, V. Bychkov^y, J. Callahan^z, D. Calvet^{aa}, M. Canneri^{ab}, M. Capeáns Garrido^h, M. Capriniⁱ, L. Cardiel Sas^h, T. Carli^h, L. Carminati^m, J. Carvalho^{ac}, M. Cascella^{ab}, M.V. Castillo^{ad}, A. Catinaccio^h, M. Cavalli Sforza^b, D. Cavalli^{ae}, V. Cavasinni^{ab}, S.A. Cetin^a, H. Chen^{af}, R. Cherkaoui^{ag}, F. Chevallier^o, M. Ciobotaru^{ah}, M. Citterio^{ae}, B. Cleland^{ai}, E. Cognerasⁿ, P. Conde Muino^{ac}, M. Consonni^m, S. Constantinescuⁱ, T. Cornelissen^h, A. Corso Radu^h, G. Costa^{ae}, P. Cwetanski^z, D. Da Silva^{aj}, M. Dam^h, H.O. Danielsson^h, D. Dannheim^h, T. Davidek^{ak}, K. De^{al}, P.O. Defay^{aa}, B. Dekhissi^{am}, J. Del Peso^{an}, M. Delmastro^h, T. Del Prete^{ab}, F. Derue^{ao}, L. Di Ciaccio^{ap}, B. Di Girolamo^h, S. Ditaⁱ, F. Dittus^h, F. Djama^{aq}, T. Djobava^{ar}, M. Dobson^h, B.A. Dolgoshein^w, A. Dotti^{ab}, G. Drake^{as}, N. Dressnandt^{at}, C. Driouchi^t, W.L. Ebenstein^q, P. Eerola^g, I. Efthymiopoulos^h, K. Egorov^z, T.F. Eifert^h, M. El Kacimi^{au}, A.I. Etienvre^x, A. Fabich^h, A.I. Fakhr-Edine^{av}, M. Fanti^m, A. Farbin^{al}, P. Farthouatⁿ, D. Fassouliotis^k, L. Fayard^u, R. Febbraro^{aa}, O.L. Fedin^{aw}, A. Fenyuk^{ax}, R. Ferrari^{ay}, B.C. Ferreira^{aj}, A. Ferrer^{ad}, G. Filippini^{aa}, D. Fournier^u, P. Francavilla^{ab}, D. Francis^h, R. Froeschl^h, D. Froidevaux^h, E. Fullana^{as}, S. Gadomski^{az}, P. Gagnon^z, S. Gameiro^h, R. Garcia^{an}, N. Ghodbane^{aa}, V. Giakoumopoulou^k, V. Giangiobbe^{ab}, N. Giokaris^k, G. Glonti^y, N. Gollub^h, A. Gomes^{ac}, M.D. Gomez^{az}, B. Gorini^h, D. Goujdami^{av}, K.J. Grahn^{ba}, P. Grenier^{bb}, N. Grigalashvili^y, Y. Grishkevich^{bc}, M. Gruwe^h, C. Guicheney^{aa}, A. Gupta^j, C. Haeblerliⁿ, Z. Hajduk^{bd}, H. Hakobyan^{be}, M. Hance^{at}, PH. Hansen^t, A. Harvey Jr.^c, A. Henriques Correia^h, L. Hervas^h, E. Higon^{ad}, J. Hoffman^{bf}, J.Y. Hostachy^o, I. Hruska^{ak}, F. Hubaut^{aq}, W. Hulsbergen^h, M. Hurwitz^j, L. Iconomidou-Fayard^u, I. Jen-La Plante^j, P.D.C. Johansson^{bg}, K. Jon-And^s, M. Joos^h, S. Jorgensen^b, A. Kaczmarska^{ao}, M. Kado^u, A. Karyukhin^{ax}, M. Kataoka^h, F. Kayumov^{bh}, A. Kazarov^{aw}, P.T. Keener^{at}, G.D. Kekelidze^y, N. Kerschen^{bg}, G. Khoraiuli^y, E. Khramov^y, A. Khristachev^{aw}, J. Khubua^y, T.H. Kittelmann^{ai}, E. Klinkby^q, T. Koffas^h, S. Kolos^{ah}, S.P. Konovalov^{bh}, S. Kopikov^{ax}, I. Korolkov^b, S. Kovalenko^{aw}, T.Z. Kowalski^{bi}, K. Krüger^h, V. Kramarenko^{bc}, L.G. Kudin^{aw}, Y. Kulchitsky^{bj}, R. Lafaye^{ap}, B. Laforge^{ao}, W. Lampl^{bk}, F. Lanni^{af}, S. Laplace^{ap}, A.C. Le Bihan^h, M. Lechowski^u, F. Ledroit-Guillon^o, G. Lehmann^h, R. Leitner^{ak}, D. Lelas^u, Z. Liang^{bf}, Z. Liang^{bl}, P. Lichard^h, M. Lokajicek^{bm}, L. Louchard^{aa}, K. Loureiro^{bn}, A. Lucotte^o, F. Luehring^z,

¹Deceased

B. Lundberg^g, B. Lund-Jensen^{ba}, H. Ma^{af}, R. Mackeprang^h, A. Maio^{ac}, V.P. Maleev^{aw}, F. Malek^o, J. Maneira^{ac}, L. Mandelli^m, M. Mazzanti^{ae}, A. Manousakis^k, L. Mapelli^h, C. Marques^{ac}, F. Martin^{at}, M. Mazzanti^{ae}, K.W. McFarlane^c, G. Mchedlidze^{ar}, R. McPherson^{bo}, C. Meirosu^h, Z. Meng^{bp}, A. Miagkov^{ax}, V. Mialkovski^y, D. Milstead^s, I. Minashvili^y, B. Mindur^{bi}, V.A. Mitsou^{ad}, E. Monnier^{aq}, S.V. Morozov^w, M. Mosidze^{ar}, S.V. Mouraviev^{bh}, A. Munar^{at}, A.V. Nadochi^{aw}, A. Negri^{ay}, S. Nemecek^{bm}, M. Nessi^h, S.Y. Nesterov^{aw}, F.M. Newcomer^{at}, I. Nikitine^{ax}, I. Nikolic-Audit^{ao}, H. Ogren^z, S.H. Oh^q, S.B. Oleshko^{aw}, J. Olszowska^{bd}, A. Onofre^{ac}, C. Padilla Aranda^h, S. Paganis^{bg}, D. Pallin^{aa}, D. Panteaⁱ, V. Paolone^{ai}, J. Parsons^{bq}, E. Pasqualucci^{br}, M.S. Passmore^h, S. Patrichev^{aw}, M. Peetz^{an}, V. Perez Reale^{bq}, L. Perini^{ae}, V.D. Peshekhonov^y, J. Petersen^h, T.C. Petersen^h, R. Petti^{bs}, J. Pilcher^l, J. Pina^{bt}, B. Pinto^{bt}, F. Podlyski^{aa}, L. Poggioli^u, J. Poveda^{bu}, P. Pralavorio^{aq}, L. Pribyl^h, M.J. Price^h, D. Prieur^{bv}, C. Puigdemont^b, P. Puzo^u, S. Rajagopalan^{af}, C. Rembser^h, M. Ridel^{ao}, I. Riu^{az}, C. Roda^{ab}, O. Rohne^{bw}, A. Romaniouk^w, D. Rousseau^u, A. Ruiz^{ad}, N. Rusakovich^y, D. Rust^z, Y.F. Ryabov^{aw}, V. Ryjov^y, O. Salto^b, B. Salvachua^{as}, C. Santamarina Rios^h, C. Santoni^{iaa}, J.G. Saraiva^{ac}, F. Sarri^{ab}, G. Sauvage^{ap}, L.P. Says^{aa}, M. Schaefer^o, V.A. Schegelsky^{aw}, G. Schlager^h, J. Schlereth^{as}, C. Schmitt^{bx}, P. Schwemling^{ao}, J. Schwindling^x, J.M. Seixas^{aj}, D.M. Seliverstov^{aw}, L. Serin^u, N. Shalanda^{by}, T. Shin^c, A. Shmeleva^{bh}, J. Silva^{ac}, S. Simion^u, M. Simonyan^{ap}, J.E. Sloper^h, S.Yu. Smirnov^w, L. Smirnova^{bc}, C. Solans^{ad}, A. Solodkov^{ax}, O. Solovianov^{ax}, I. Soloviev^{aw}, V.V. Sosnovtsev^w, F. Spanò^{bq}, P. Speckmeyer^h, S. Stancu^{ah}, R. Stanek^{as}, E. Starchenko^{ax}, A. Straessner^{bz}, S.I. Suchkov^w, M. Suk^{ak}, R.R. Szczygiel^{bd}, F. Tarrade^{af}, F. Tartarelli^{ae}, P. Tas^{ak}, Y. Tayalati^{aa}, R. Teuscher^{ca}, M. Thioye^f, V.O. Tikhomirov^{bh}, S. Tisserant^{aq}, L. Tremblet^h, P. Tsiareshka^{bj}, G. Unal^h, G. Unel^z, G. Usai^j, A. Valero^{ad}, S. Valkar^{ak}, J.A. Valls^{ad}, R. Van Berg^{at}, W. Vandelli^h, F. Vannucci^{ao}, A. Vartapetian^{al}, V.I. Vassilikopoulos^c, L. Vassilieva^{bh}, F. Vazeille^{aa}, Y. Vetter-Cole^{bf}, I. Vichou^{cb}, V. Vinogradov^y, I. Vivarelli^{ab}, M. Volpi^b, C. Wang^q, P. Werner^h, S. Wheeler^{cc}, M. Wiesmann^h, H. Wilkens^h, H.H. Williams^{at}, I. Wingerter-Seez^{ap}, Y. Yasu^{cd}, A. Zaitsev^{ax}, A. Zenin^{ax}, T. Zenis^{ce}, Z. Zenonos^{ab}, H. Zhang^{aq}, N. Zhou^{bq}

^aBogazici University, Faculty of Sciences, Department of Physics, TR - 80815 Bebek-Istanbul, Turkey

^bInstitut de Fisica d'Altes Energies, IFAE, Universitat Autònoma de Barcelona, Edifici Cn, ES - 08193 Bellaterra (Barcelona) Spain

^cHampton University, Department of Physics, Hampton VA 23668, United States of America

^dQueen Mary, University of London, Mile End Road, E1 4NS, London, United Kingdom

^eUniversität Mainz, Institut fuer Physik, Staudinger Weg 7, DE 55099, Germany

^fDepartment of Physics and Astronomy, Stony Brook, NY 11794-3800, United States of America

^gLunds universitet, Naturvetenskapliga fakulteten, Fysiska institutionen, Box 118, SE - 221 00, Lund, Sweden

^hEuropean Laboratory for Particle Physics (CERN), CH-1211 Geneva 23, Switzerland

ⁱNational Institute of Physics and Nuclear Engineering (Bucharest -IFIN-HH), P.O. Box MG-6, R-077125 Bucharest, Romania

^jUniversity of Chicago, Enrico Fermi Institute, 5640 S. Ellis Avenue, Chicago, IL 60637, United States of America

^kUniversity of Athens, Nuclear & Particle Physics Department of Physics, Panepistimiopouli Zografou, GR 15771 Athens, Greece

^lYale University, Department of Physics, PO Box 208121, New Haven, CT06520-8121, United States of America

^mUniversità di Milano, Dipartimento di Fisica and INFN, via Celoria 16, IT - 20133 Milano, Italy

- ⁿUniversity of Bern, Laboratory for High Energy Physics, Sidlerstrasse 5, CH - 3012 Bern, Switzerland
- ^oLaboratoire de Physique Subatomique et de Cosmologie CNRS/IN2P3, Université Joseph Fourier INPG, 53 avenue des Martyrs, FR - 38026 Grenoble Cedex, France
- ^pUniversité Hassan II, Faculté des Sciences Ain Chock, B.P. 5366, MA - Casablanca, Morocco
- ^qDuke University, Department of Physics Durham, NC 27708, United States of America
- ^rUniversity of Regina, Physics Department, Canada
- ^sStockholm University, Department of Physics, SE - 106 91 Stockholm, Sweden
- ^tUniversity of Copenhagen, Niels Bohr Institute, Blegdamsvej 17, DK - 2100 Kobenhavn 0, Denmark
- ^uLAL, Université Paris-Sud, IN2P3/CNRS, Orsay, France
- ^vCentre de Calcul CNRS/IN2P3, Lyon, France
- ^wMoscow Engineering & Physics Institute (MEPhI), Kashirskoe Shosse 31, RU 115409 Moscow, Russia
- ^xCommissariat à l'Energie Atomique (CEA), DSM/DAPNIA, Centre d'Etudes de Saclay, 91191 Gif-sur-Yvette, France
- ^yJoint Institute for Nuclear Research, JINR Dubna, RU - 141 980 Moscow Region, Russia
- ^zIndiana University, Department of Physics, Swain Hall West 117, Bloomington, IN 47405-7105, United States of America
- ^{aa}Laboratoire de Physique Corpusculaire (LPC), IN2P3-CNRS, Université Blaise-Pascal Clermont-Ferrand, FR - 63177 Aubiere, France
- ^{ab}Università di Pisa, Dipartimento di Fisica E. Fermi and INFN Pisa, Largo B. Pontecorvo 3, IT - 56127 Pisa, Italy
- ^{ac}Laboratorio de Instrumentacao e Fisica Experimental de Particulas, LIP, Avenida Elias Garcia 14-1, PT - 1000-149 Lisboa, Portugal
- ^{ad}Univ. of Valencia, Centro Mixto UVEG-CSIC, Instituto de Fisica Corpuscular (IFIC), Apdo. 22085 ES-46071 Spain
- ^{ae}INFN Sezione di Milano, via Celoria 16, IT - 20133 Milano, Italy
- ^{af}Brookhaven National Laboratory, Physics Department, Bldg. 510A Upton S, NY 11973, United States of America
- ^{ag}Université Mohammed V, Faculté des Sciences, BP 1014, MO - Rabat, Morocco
- ^{ah}University of California, Department of Physics & Astronomy, Irvine, CA 92697-4575, United States of America
- ^{ai}University of Pittsburgh, Department of Physics and Astronomy, 3941 O'Hara Street, Pittsburgh, PA 15260, United States of America
- ^{aj}Universidade Federal do Rio De Janeiro, Instituto de Fisica, Caixa Postal 68528, Ilha do Fundao, BR - 21945-970 Rio de Janeiro, Brazil
- ^{ak}Charles University in Prague, Faculty of Mathematics and Physics, Institute of Particle and Nuclear Physics, V Holesovickach 2, CZ - 18000 Praha 8, Czech Republic
- ^{al}University of Texas at Arlington, Department of Physics, Box 19059, Arlington, TX 76019, United States of America
- ^{am}Laboratoire de Physique Théorique et de Physique des Particules, Université Mohammed Premier, Oujda, Morocco
- ^{an}Universidad Autonoma de Madrid, Facultad de Ciencias, Departamento de Fisica Teorica, ES - 28049 Madrid, Spain
- ^{ao}Université Pierre et Marie Curie (Paris 6) and Université Denis Diderot (Paris-7), Laboratoire de Physique Nucléaire et de Hautes Energies, CNRS/IN2P3, Tour 33 4 place Jussieu, FR - 75252 Paris Cedex 05, France
- ^{ap}Laboratoire de Physique de Particules (LAPP), Université de Savoie, CNRS/IN2P3, Annecy-le-Vieux Cedex, France
- ^{aq}Université Méditerranée, Centre de Physique des Particules de Marseille, CNRS/IN2P3, F-13288 Marseille, France
- ^{ar}Tbilisi State University, High Energy Physics Institute, University St. 9, GE - 380086 Tbilisi, Georgia
- ^{as}Argonne National Laboratory, High Energy Physics Division, 9700 S. Cass Avenue, Argonne IL 60439, United States of America
- ^{at}University of Pennsylvania, Department of Physics, High Energy Physics, 209 S. 33rd Street Philadelphia, PA 19104, United States of America
- ^{au}Laboratoire de Physique de Particules (LAPP), Université de Savoie, CNRS/IN2P3, Annecy-le-Vieux Cedex, France and Université Cadi Ayyad, Marrakech, Morocco
- ^{av}Université Cadi Ayyad, Marrakech, Morocco

- ^{aw} Petersburg Nuclear Physics Institute, RU - 188 300 Gatchina, Russia
- ^{ax} Institute for High Energy Physics (IHEP), Federal Agency of Atom. Energy, Moscow Region, RU - 142 284 Protvino, Russia
- ^{ay} Università di Pavia, Dipartimento di Fisica Nucleare e Teorica and INFN Pavia, Via Bassi 6 IT-27100 Pavia, Italy
- ^{az} Université de Genève, Section de Physique, 24 rue Ernest Ansermet, CH - 1211 Genève 4, Switzerland
- ^{ba} Royal Institute of Technology (KTH), Physics Department, SE - 106 91 Stockholm, Sweden
- ^{bb} SLAC National Accelerator Laboratory, Stanford, California 94309, United States of America
- ^{bc} Lomonosov Moscow State University, Skobeltsyn Institute of Nuclear Physics, RU - 119 991 GSP-1 Moscow Lenskiyegory 1-2, Russia
- ^{bd} The Henryk Niewodniczanski Institute of Nuclear Physics, Polish Academy of Sciences, ul. Radzikowskiego 152, PL - 31342 Krakow Poland
- ^{be} Yerevan Physics Institute, Alikhanian Brothers Street 2, AM - 375036 Yerevan, Armenia
- ^{bf} Southern Methodist University, Physics Department, 106 Fondren Science Building, Dallas, TX 75275-0175, United States of America
- ^{bg} University of Sheffield, Department of Physics & Astronomy, Hounseld Road, Sheffield S3 7RH, United Kingdom
- ^{bh} P.N. Lebedev Institute of Physics, Academy of Sciences, Leninsky pr. 53, RU - 117 924, Moscow, Russia
- ^{bi} University of Science and Technology, Faculty of Physics and Applied Computer Science of (FPACS AGH-UST), al. Mickiewicza 30, PL-30059 Cracow, Poland
- ^{bj} B.I. Stepanov Institute of Physics, National Academy of Sciences of Belarus, Independence Avenue 68, Minsk 220072, Republic of Belarus and Joint Institute for Nuclear Research, JINR Dubna, RU - 141 980 Moscow Region, Russia
- ^{bk} University of Arizona, Department of Physics, Tucson, AZ 85721, United States of America
- ^{bl} Institute of Physics, Academia Sinica, TW - Taipei 11529, Taiwan and Sun Yat-sen University, School of physics and engineering, Guangzhou 510275, P. R. China
- ^{bm} Academy of Sciences of the Czech Republic, Institute of Physics and Institute for Computer Science, Na Slovance 2, CZ - 18221 Praha 8, Czech Republic
- ^{bn} Ohio State University, 191 West Woodruff Ave, Columbus, OH 43210-1117, United States of America
- ^{bo} University of Victoria, Department of Physics and Astronomy, P.O. Box 3055, Victoria B.C., V8W 3P6, Canada
- ^{bp} Institute of Physics, Academia Sinica, TW - Taipei 11529, Taiwan and Shandong University, School of Physics, Jinan, Shandong 250100, P. R. China
- ^{bq} Columbia University, Nevis Laboratory, 136 So. Broadway, Irvington, NY 10533, United States of America
- ^{br} Università La Sapienza, Dipartimento di Fisica and INFN Roma I, Piazzale A. Moro 2, IT- 00185 Roma, Italy
- ^{bs} University of South Carolina, Columbia, United States of America
- ^{bt} LIP and IDMEC-IST, Lisboa, Portugal
- ^{bu} University of Wisconsin, Department of Physics, 1150 University Avenue, WI 53706 Madison, Wisconsin, United States of America
- ^{bv} Rutherford Appleton Laboratory, Science and Technology Facilities Council, Harwell Science and Innovation Campus, Didcot OX11 0QX, United Kingdom
- ^{bw} University of Oslo, Department of Physics, P.O. Box 1048, Blindern T, NO - 0316 Oslo, Norway
- ^{bx} University of Bonn, Physikalisches Institut, Nussallee 12, D - 53115 Bonn, Germany
- ^{by} B.I. Stepanov Institute of Physics, National Academy of Sciences of Belarus, Independence Avenue 68, Minsk 220072, Republic of Belarus
- ^{bz} Technical University Dresden, Institut fuer Kern- und Teilchenphysik, Zellescher Weg 19, D-01069 Dresden, Germany
- ^{ca} University of Toronto, Department of Physics, 60 Saint George Street, Toronto M5S 1A7, Ontario, Canada
- ^{cb} University of Illinois, Department of Physics, 1110 West Green Street, Urbana, Illinois 61801 United States of America
- ^{cc} University of Alberta, Department of Physics, Centre for Particle Physics, Edmonton, AB T6G 2G7, Canada
- ^{cd} KEK, High Energy Accelerator Research Organization, 1-1 Oho Tsukuba-shi, Ibaraki-ken 305-0801, Japan

Abstract

A fully instrumented slice of the ATLAS detector was exposed to test beams from the SPS (Super Proton Synchrotron) at CERN in 2004. In this paper, the results of the measurements of the response of the central calorimeter to hadrons with energies in the range 20 to 350 GeV and beam impact points and angles corresponding to pseudo-rapidity values in the range 0.2-0.65 are reported. The results are compared to the predictions of a simulation program using the Geant 4 toolkit.

Keywords: ATLAS, calorimetry, test-beam, calibration, simulation

PACS: 29.40.Vj

1. Introduction

2 In 2004 a ATLAS Combined Test Beam (CTB) program was carried out at CERN.
3 A slice of the detector composed of the final versions of all central sub-detectors was
4 exposed to the SPS (Super Proton Synchrotron) beams. The layout of the sub-detectors
5 was designed to be as close as possible to that of ATLAS. The Data Acquisition system
6 (DAQ) [1] was also similar to the one being used in ATLAS.

7 The calorimeter system in ATLAS consists of an electromagnetic (LAr) and a
8 hadronic calorimeter (TileCal). It will be used to measure the energy of jets over a
9 wide energy range, from about 20 GeV to more than 1 TeV. In this paper, the measure-
10 ment of the combined response of the barrel calorimeter to hadron beams with energies
11 in the range 20 to 350 GeV is presented. It was performed for various incident angles
12 corresponding to pseudo-rapidity values $\eta_{beam} = 0.20, 0.25, 0.35, 0.45, 0.55$ and 0.65.
13 The response of TileCal to hadrons that start showering after the LAr calorimeter was
14 also determined. The results were compared to the predictions of the Monte Carlo
15 (MC) simulation program Geant 4 [2, 3, 4]. The agreement between the data and the
16 simulation results is discussed. Results obtained using pions of energy from 3 to 9 GeV
can be found in Ref. [5].

18 2. The experimental set-up

2.1. The beam line

20 The beams were produced by extracting 400 GeV protons from the Super Proton
21 Synchrotron (SPS) machine towards the North Area [6]. The primary target made of
22 beryllium had a length of 300 mm. The produced secondary beams can have ener-
23 gies from 10 to 350 GeV. A secondary filter target of 1000 mm of polyethylene plus
24 lead absorber can be placed in the beam to produce tertiary beams. Bending magnets
were used to determine the beam momentum and charge. The beams are expected to

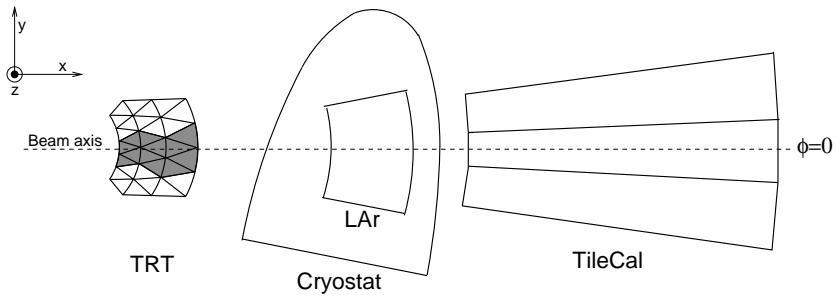


Figure 1: Beam line detectors layout.

26 be composed mainly of pions and, in the case of beams of positive charge, protons.
 27 Electrons and muons are also present. The results reported in this paper were obtained
 28 using positive (negative) beams with energies equal to 20, 50 and 100 (150, 180, 200,
 250, 320 and 350) GeV.

30 The transverse beam profile was monitored by three wire chambers (BC0, BC1
 and BC2) [7]. Two scintillators, with an active surface of $5 \times 5 \text{ cm}^2$ [8] were used in
 32 coincidence to trigger the DAQ (Physics Trigger) and to provide the trigger timing.
 These two detectors together with the scintillator S1 were used to reject beam particles
 34 interacting upstream of the detectors. A scintillation counter (MTS) was placed after
 the detector, behind an absorber, to identify beam muons. In this paper we will use
 36 a right-handed coordinate system with the x-axis along the beam line and the y-axis
 pointing up, see Figure 1.

38 2.2. The detector

Figure 1 shows a side-view of the layout of the ATLAS sub-detectors during the
 40 2004 CTB. Only sub-detectors that were used in the present analysis are shown. The
 ATLAS Inner Detector (ID) [9] consists of three systems: the Silicon Pixel Detector,
 42 the Semi-Conductor Tracker (SCT) and the Transition Radiation Tracker (TRT).
 Modules of such detectors were placed in front of the calorimeters but they were not
 44 operational during the considered data taking period. The TRT module is shown in Fig.
 1 because the measurements performed with this detector in other occasions allowed
 46 the determinations of the pion-proton mixings in the case of positive beams [10].

The LAr module [11, 12] is made out of accordion-shaped lead absorbers glued
 48 between two stainless steel sheets and placed inside a cryostat, made of aluminum,
 containing liquid argon. Beam entrance and exit walls are each 0.2 interaction lengths
 50 (λ) thick. The calorimeter has four longitudinal layers, including a pre-sampler. The
 coverage of all four layers is $0 < \eta < 1.4$ and $-\pi/16 < \phi < \pi/16$ rad (see Figs 1 and
 52 2 for ϕ and η orientation convention). The $\eta - \phi$ granularity of each longitudinal layer
 is described in [11].

54 Three modules of TileCal were exposed to the beams [13]. The iron-scintillator
 media of the modules is made of 4 and 5 mm thick iron plates sandwiched by 3 mm
 56 thick scintillator tiles, with a periodicity of 18 mm. The TileCal modules were placed

about 30 cm behind the LAr calorimeter.² The total coverage of the subdetector was
58 $-1 < \eta < 1$ and $-3\pi/64 < \phi < 3\pi/64$ rad. Each TileCal module has 3 longitudinal
layers, whose $\eta - \phi$ granularity is described in [13] (see also Figure 2). LAr and
60 TileCal were both supported by a mobile table. This table was oriented in such a way
that the incoming particles in the calorimeters were projective in pseudo-rapidity as in
62 the ATLAS experiment.

Various sections of the ATLAS muon spectrometer [14] were also present in the
64 2004 CTB set-up. This sub-detector has not been used for the analysis presented in
this paper.

66 3. Data sets and event selections

In this section the requirements applied to select events produced by collimated
hadrons that do not strongly interact in the beam line before reaching the LAr calorime-
ter are discussed. The cuts on the beam line scintillating counters signals: E_{S1} , E_{S2} ,
 $E_{S3right}$ and E_{S3left} were established studying the responses of S1, S2 and S3 to muons.
Muon events were recognized by requiring a signal above the pedestal level in the
MTS counter. The scintillator S3 was read by two photomultipliers labeled left and
right. The following selections were applied (cut 1):

$$E_{S1} < 2 \times peak_{S1}^{muon} \quad (1)$$

$$E_{S2} < 2 \times peak_{S2}^{muon}$$

$$E_{S3right} < 2 \times peak_{S3right}^{muon}$$

$$E_{S3left} < 2 \times peak_{S3left}^{muon}.$$

The quantities $peak_{S1}^{muon}$, $peak_{S2}^{muon}$, $peak_{S3right}^{muon}$ and $peak_{S3left}^{muon}$ are the most probable
68 values of the muon distributions after pedestal subtraction.

The beam chambers BCn (n = 0, 1 and 2) allow a determination of the transversal
beam impact point coordinates: y_{BCn} and z_{BCn} . The accepted events satisfy in each
chamber n the conditions (cut 2):

$$\mu_{BCn}(y) - 2\sigma_{BCn}(y) < y_{BCn} < \mu_{BCn}(y) + 2\sigma_{BCn}(y) \quad (2)$$

$$\mu_{BCn}(z) - 2\sigma_{BCn}(z) < z_{BCn} < \mu_{BCn}(z) + 2\sigma_{BCn}(z).$$

The Gaussian functions means, $\mu_{BCn}(y)$ and $\mu_{BCn}(z)$ and sigmas, $\sigma_{BCn}(y)$ and
70 $\sigma_{BCn}(z)$ were obtained by fitting such functions to the data. The sigma values are
about 30 mm and differ slightly from run to run.

The divergence of the beam was estimated using the differences of the impact point
coordinates in the chambers BC₀, BC₁ and BC₂: $\Delta_{(0,1)}(y) = y_{BC0} - y_{BC1}$, $\Delta_{(1,2)}(y) =$

²In ATLAS this distance is 25 cm.

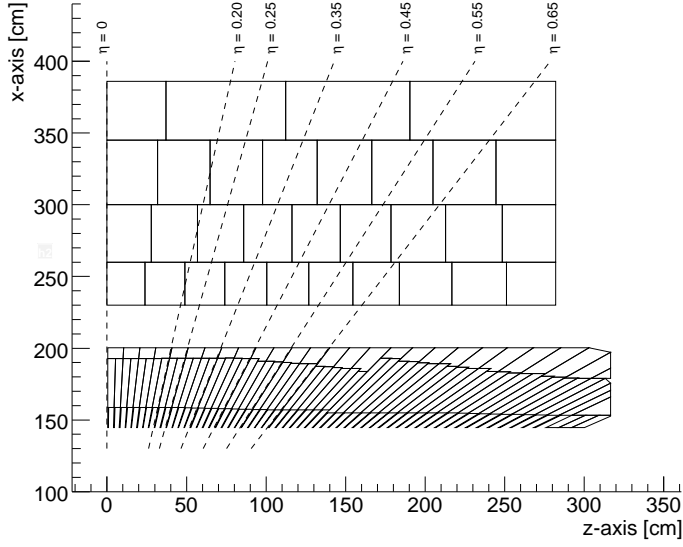


Figure 2: Top view of the calorimeters layout in the 2004 CTB. The TileCal modules are only represented for $\eta > 0$.

$y_{BC1} - y_{BC2}$, $\Delta_{(0,1)}(z) = z_{BC0} - z_{BC1}$ and $\Delta_{(1,2)}(z) = z_{BC1} - z_{BC2}$. The retained events satisfy the conditions (cut 3):

$$\begin{aligned}
 \mu_{\Delta(0,1)}(y) - 2\sigma_{\Delta(0,1)n}(y) &< \Delta_{(0,1)}(y) < \mu_{\Delta(0,1)}(y) + 2\sigma_{\Delta(0,1)n}(y) & (3) \\
 \mu_{\Delta(1,2)}(y) - 2\sigma_{\Delta(1,2)n}(y) &< \Delta_{(1,2)}(y) < \mu_{\Delta(1,2)}(y) + 2\sigma_{\Delta(1,2)n}(y) \\
 \mu_{\Delta(0,1)}(z) - 2\sigma_{\Delta(0,1)n}(z) &< \Delta_{(0,1)}(z) < \mu_{\Delta(0,1)}(z) + 2\sigma_{\Delta(0,1)n}(z) \\
 \mu_{\Delta(1,2)}(z) - 2\sigma_{\Delta(1,2)n}(z) &< \Delta_{(1,2)}(z) < \mu_{\Delta(1,2)}(z) + 2\sigma_{\Delta(1,2)n}(z).
 \end{aligned}$$

72 The symbols $\mu_{\Delta(0,1)}(y)$, $\mu_{\Delta(1,2)}(y)$, $\mu_{\Delta(0,1)}(z)$ and $\mu_{\Delta(1,2)}(z)$ and $\sigma_{\Delta(0,1)n}(y)$, $\sigma_{\Delta(1,2)n}(y)$,
 74 $\sigma_{\Delta(0,1)n}(z)$ and $\sigma_{\Delta(1,2)n}(z)$ indicate the mean and sigma values of Gaussian functions fitting the distributions.

At the energies considered, electrons impinging in the calorimeter, deposit essentially all their energy in the LAr. In the case of hadrons, a large fraction of the energy is deposited in TileCal. Electrons were then rejected requiring (cut 4):

$$\frac{E_{raw}(LAr)}{E_{raw}(LAr) + E_{raw}(TileCal)} < 0.98 \quad (4)$$

76 The residual electron contamination was estimated to be negligible for all the energies.

78 The methods used to reconstruct the energies deposited in LAr ($E_{raw}(LAr)$) and TileCal ($E_{raw}(TileCal)$) are discussed in Section 4.

E_{nom} [GeV]	50	150	250	350
Physics Trigger (Section 2.1)	47232	81071	7150	21894
Cut 1: Beam line scintillator	42608	76662	5893	17993
Cut 2: Beam chambers impact point	39405	66371	5483	17175
Cut 3: Beam chambers divergence	31263	52724	4509	13417
Cut 4: $\frac{E_{raw}(LAr)}{E_{raw}(LAr)+E_{raw}(TileCal)} < 0.98$	29327	51848	4438	13337
Cut 5: $E_{MTS} < 500$ [ADC channels]	28427	22243	4390	13106
Cut 6: $E_{raw}(Total) > 6$ GeV	28123	22189	4390	13104
Cut 7: Small energy deposition in LAr	4936	4233	870	2512

Table 1: Number of events retained after each individual selection requirement for data collected using incident beams at $\eta=0.45$. The corresponding nominal beam energy values are reported.

Muon events were rejected by requiring a signal in the MTS counter compatible with noise (cut 5):

$$E_{MTS} < 500 [\text{ADC channels}]. \quad (5)$$

The mean energy deposited in the calorimeter by muons is much smaller than the one deposited by hadrons. A further rejection was then obtained requiring (cut 6):

$$E_{raw}(LAr) + E_{raw}(TileCal) > 6 [\text{GeV}]. \quad (6)$$

The cuts 1-6 allowed selecting clean hadron showers in the calorimeter (Sample 1). Hadrons showering in TileCal (Sample 2) were obtained by further requiring a small energy deposition in LAr. For each of the three LAr layers i , the measured energy $E_{raw}^i(LAr)$ must satisfy the condition (cut 7):

$$E_{raw}^i(LAr) < \mu_{LAr}^i(muon) + 2 \times \sigma_{LAr}^i(muon). \quad (7)$$

The quantities $\mu_{LAr}^i(muon)$ and $\sigma_{LAr}^i(muon)$ in eq. (7) are the mean values and the root mean square of the $E_{raw}^i(LAr)$ distributions obtained using muon events.

In the following the results obtained analyzing Sample 1 (Sample 2) events will be labeled Comb (TileCal). In Table 1 the numbers of events passing the selection criteria are reported. The beams have nominal energies equal to 50, 150, 250 and 350 GeV and $\eta_{beam} = 0.45$. All other runs show similar cut efficiencies, demonstrating a satisfactory stability of the beam conditions and of the detector operations during the data taking. The number of the selected Sample 1 (Sample 2) events are a few thousands (tens of thousands). The positive beam samples at 20, 50 and 100 GeV contain pions and protons. The fractions of pions and protons in the hadron beams and their effects on the results are discussed in section 6. The other samples contain only pions.

4. Reconstruction of the energy in the calorimeters

4.1. Cell energy reconstruction

The cell energy in LAr is determined by the Optimal Filtering Coefficients Method [15, 16]. The comparison of the measured and simulated energy response of 180 GeV

94 electrons allowed the determination of the energy scale. The uncertainty on the scale,
 due mainly to the knowledge of the beam momentum [16], is 0.7%. In TileCal, the fit
 96 filter method is used to determine the cell energy [17]. The scale of the reconstructed
 energy was obtained using electron beams incident at the center of each cell with an
 98 angle of 20° . The estimated uncertainty on the energy scale is 0.5% [17].

4.2. The reconstructed energies

In the case of Sample 1 selected events, the combined reconstructed shower energy was obtained using the formula

$$E_{raw}^{Comb} = E_{raw}(LAr) + E_{raw}(TileCal). \quad (8)$$

For Sample 2 events one has:

$$E_{raw}^{TileCal} = E_{raw}(TileCal). \quad (9)$$

The quantities $E_{raw}(LAr)$ and $E_{raw}(TileCal)$ are, respectively, the sums of the energy deposited in the LAr and TileCal calorimeter cells having pseudo-rapidity coordinates η_{cell} satisfying the condition $\eta_{beam} - 0.20 \leq \eta_{cell} \leq \eta_{beam} + 0.20$. In the case of LAr only, the cells of the three layers have been used. No corrections for dead material, containment and non-compensation effects were applied. In order to improve the energy resolution, only cells with an energy E_{cell} larger than twice the standard deviation of the residual electronic noise σ_{noise} (in absolute value) were considered in the sums:

$$|E_{cell}| > 2 \times \sigma_{noise}. \quad (10)$$

100 4.3. The electronic noise

The standard deviation σ_{noise} of the electronic noise distribution varies from cell to
 102 cell, with large variations between different longitudinal layers. For each run, σ_{noise} has
 been determined for each cell of the calorimeter using pedestal events obtained from
 104 random triggers between beam bursts. Typical σ_{noise} values are 12 MeV (1st layer of
 LAr), 28 MeV (2nd layer of LAr), 22 MeV (3rd layer of LAr), 30 MeV (1st layer of
 106 TileCal), 30 MeV (2nd layer of TileCal) and 25 MeV (3rd layer of TileCal). The typical
 number of cells considered in the computation of the energy in the calorimeter is about
 108 160. The electronic noise has a negligible effect on the resolution of the hadron energy
 measurements (see Section 5.2).

110 Pedestal levels of the calorimeter cells were studied. In the case of LAr, special
 runs were taken every eight hours during the data taking. For each cell and electronic
 112 gain setting, pedestals were recorded in each of the seven time windows in which the
 cell pulse is sampled. The mean pedestal in a cell was obtained as the average of the
 114 seven measurements. Corrections were also applied to take into account the drift due
 to changes of the temperature of the electronic front-end boards during the data-taking.
 116 The typical size of these corrections on the reconstructed energies is about 10 MeV
 [15, 16].

118 In the case of TileCal the fit method applied to reconstruct the cell energy uses an
 event-by-event baseline subtraction and therefore corrects for any pedestal shifts. The

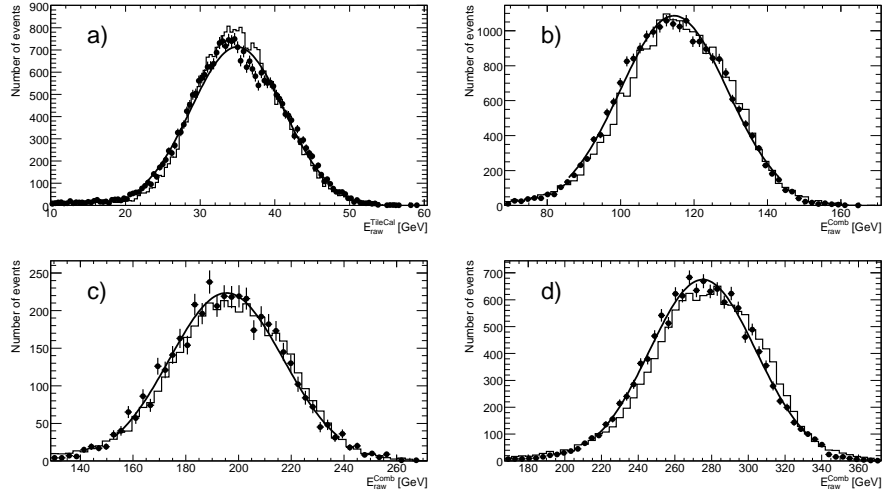


Figure 3: Distribution of the reconstructed energy E_{raw}^{Comb} (see Eq. (8)) obtained for E_{nom} equal to (a) 50 GeV, (b) 150 GeV, (c) 250 GeV and (d) 350 GeV, and $\eta=0.45$. The full points represent the experimental data. The solid curves correspond to the fit of a Gauss function to the data (see the text). The histograms correspond to the prediction of the Monte Carlo simulation (Section 6).

120 residual effect on the reconstructed energy was estimated to be about 6 MeV. These
 122 effects are negligible in comparison to the typical reconstructed hadron energy uncer-
 tainty (See Section 5).

124 Out of a total of about 2000 channels no dead or hot LAr and TileCal channels were
 found during the data taking.

5. Calorimeter response to hadrons

126 5.1. Determination of the hadron response

The response has been measured for hadron samples at various energies and pseudo-
 128 rapidities. Figure 3 shows the energy deposit E_{raw}^{Comb} distributions in the ATLAS calorime-
 130 ter system when the hadron beam impinged on the calorimeter at $\eta=0.45$ and for
 hadrons of nominal energies $E_{nom}= 50, 150, 250$ and 350 GeV. Figure 4 shows the
 energy deposit in the case of hadrons showering after LAr. The beam parameters are
 132 the same as Figure 3.

The distributions are described reasonably well by Gaussian functions. The res-
 134 sponses E^{Comb} ($E^{TileCal}$) and resolution σ^{Comb} ($\sigma^{TileCal}$) were then defined as the μ
 and σ parameters of such function fitting the measured distributions in a region $\pm 2\sigma$'s
 136 around the mean value.³ The fit functions are superimposed to the data distributions of
 Figures 3 and 4. The results are reported in Tables 2 and 3.

³An iterative procedure has been applied in order to get stable values of the parameters.

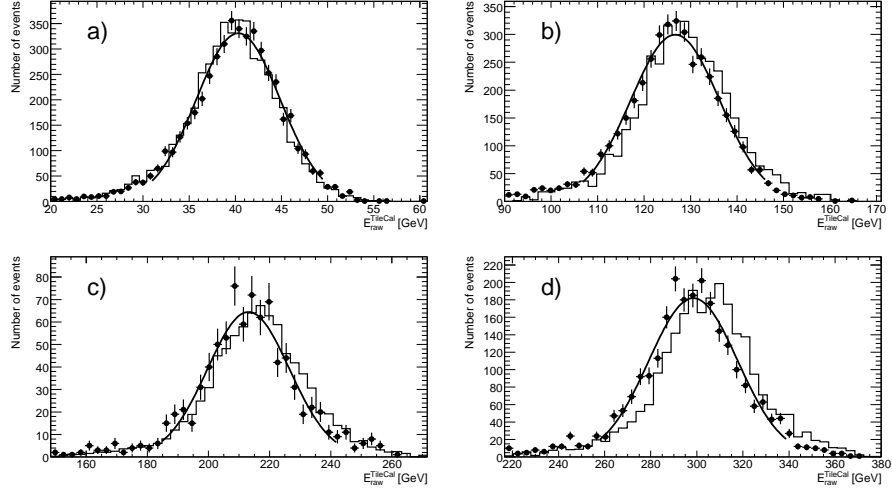


Figure 4: Distribution of the reconstructed energy $E_{raw}^{TileCal}$ (see Eq. (9)) obtained for E_{nom} equal to (a) 50 GeV, (b) 150 GeV, (c) 250 GeV and (d) 350 GeV, and $\eta=0.45$. The full points represent the experimental data. The solid curves correspond to the fit of a Gauss function to the data (see the text). The histograms correspond to the prediction of the Monte Carlo simulation (Section 6).

138 5.2. Measurements of the energy response ratios and of the fractional resolutions

The measurements of the energy response ratios, $R^{E^{Comb}} = E^{Comb} / E_{beam}$ and $R^{E^{TileCal}} = E^{TileCal} / E_{beam}$, are reported in Tables 4 and 5 respectively. The quantity E_{beam} is the beam energy determined using beam line magnet measurements [6]. The differences between E_{beam} and E_{nom} were measured to be smaller than 1%. The effects of the ID material in front of LAr were estimated using few runs at $\eta=0.45$ with ID detectors operational. A correction of +1% was applied to the values of the energy response ratios. The values of energy response ratios are $\cong 65\%$ ($\cong 75\%$) at 20 GeV and $\cong 78\%$ ($\cong 86\%$) at 350 GeV.

In the tables statistical and the systematic uncertainties were combined in quadrature. Three sources of systematic uncertainty were considered:

- i the uncertainty on the LAr (Δ_{scale}^{LAr}) and TileCal ($\Delta_{scale}^{TileCal}$) energy scale
- 150 ii the non uniformity of the LAr ($\Delta_{uniformity}^{LAr}$) and TileCal ($\Delta_{uniformity}^{TileCal}$) energy response
- iii the effect of the ID material in front of LAr.

152 Variations obtained applying different selection criteria were found to be negligible. The systematic uncertainties (i) are discussed in section 4.1. They affect in a correlated way the energy response ratio determinations of the different data points.

The non-uniformity of the LAr and TileCal response was studied using pion beams. 156 The obtained numerical values are $\Delta_{uniformity}^{LAr} = 0.4\%$ [15, 16] and $\Delta_{uniformity}^{TileCal} = 1.5\%$ [17]. The corresponding uncertainty values on the determinations of the energy response ratios, $\Delta(R^{E^{Comb}})_{unif}$ and $\Delta(R^{E^{TileCal}})_{unif}$, are correlated in the case of the data 158

E_{nom} [GeV]	$\eta_{beam} = 0.20$		$\eta_{beam} = 0.25$		$\eta_{beam} = 0.35$	
	E^{Comb} [GeV]	σ^{Comb} [GeV]	E^{Comb} [GeV]	σ^{Comb} [GeV]	E^{Comb} [GeV]	σ^{Comb} [GeV]
20	12.97±0.03	3.52±0.03	13.10±0.03	3.27±0.03	12.99±0.03	3.26±0.03
50	34.56±0.06	6.94±0.06	34.14±0.07	6.20±0.07	34.99±0.06	6.09±0.06
100	-	-	73.29±0.08	9.83±0.08	72.7±0.1	9.8±0.1
150	116.3±0.2	16.7±0.2	115.5±0.1	14.2±0.1	115.1±0.1	14.5±0.1
180	141.1±0.1	19.5±0.1	139.9±0.2	16.1±0.1	139.2±0.2	17.0±0.2
200	156.9±0.2	21.1±0.2	155.9±0.2	17.9±0.2	155.0±0.2	18.2±0.2
250	193.6±0.2	24.9±0.1	192.6±0.2	21.7±0.2	-	-
320	244.3±0.4	32.4±0.4	246.8±0.3	26.6±0.3	243.6±0.4	26.7±0.4
350	272.2±0.3	34.7±0.3	271.8±0.3	28.5±0.3	272.1±0.3	28.6±0.3
E_{nom} [GeV]	$\eta_{beam} = 0.45$		$\eta_{beam} = 0.55$		$\eta_{beam} = 0.65$	
	E^{Comb} [GeV]	σ^{Comb} [GeV]	E^{Comb} [GeV]	σ^{Comb} [GeV]	E^{Comb} [GeV]	σ^{Comb} [GeV]
20	12.90±0.03	3.21±0.03	12.79±0.03	3.30±0.03	12.35±0.03	3.31±0.03
50	34.96±0.04	6.22±0.04	34.75±0.06	6.38±0.06	33.83±0.05	6.54±0.05
100	72.51±0.06	10.01±0.06	72.0±0.1	10.29±0.08	70.41±0.09	10.76±0.08
150	114.5±0.1	14.7±0.1	114.5±0.2	15.4±0.2	112.5±0.2	16.1±0.2
180	137.0±0.1	17.3±0.1	137.9±0.2	17.8±0.2	136.5±0.2	18.5±0.2
200	152.1±0.1	18.6±0.1	154.1±0.2	19.0±0.2	152.4±0.2	20.4±0.2
250	195.4±0.4	21.6±0.4	-	-	-	-
320	246.3±0.4	27.3±0.4	-	-	239.2±0.5	30.8±0.5
350	275.2±0.3	29.1±0.3	275.2±0.3	29.6±0.3	270.3±0.3	31.7±0.3

Table 2: Measured energy response E^{Comb} and resolution σ^{Comb} for different values of the nominal beam energy and η_{beam} . Only statistical uncertainties are reported.

E_{nom} [GeV]	$\eta_{beam} = 0.20$		$\eta_{beam} = 0.25$		$\eta_{beam} = 0.35$	
	$E^{TileCal}$ [GeV]	$\sigma^{TileCal}$ [GeV]	$E^{TileCal}$ [GeV]	$\sigma^{TileCal}$ [GeV]	$E^{TileCal}$ [GeV]	$\sigma^{TileCal}$ [GeV]
20	15.46±0.06	3.18±0.06	15.15±0.05	2.74±0.05	15.22±0.06	2.84±0.07
50	41.2±0.1	5.8±0.1	40.4±0.1	4.5±0.1	40.4±0.1	4.5±0.1
100	-	-	82.2±0.1	6.9±0.1	81.9±0.2	7.2±0.2
150	132.5±0.2	11.4±0.2	126.5±0.2	9.5±0.2	127.3±0.2	9.7±0.2
180	158.8±0.2	13.8±0.2	152.7±0.2	10.9±0.2	153.3±0.2	11.1±0.2
200	177.0±0.2	15.3±0.3	170.1±0.3	12.8±0.3	170.5±0.2	12.3±0.2
250	219.9±0.2	17.7±0.2	213.6±0.3	15.3±0.3	-	-
320	275.6±0.6	23.6±0.6	269.5±0.4	18.9±0.4	269.2±0.6	17.8±0.6
350	304.6±0.4	25.2±0.4	296.2±0.4	20.0±0.4	297.2±0.4	19.5±0.4
E_{nom} [GeV]	$\eta_{beam} = 0.45$		$\eta_{beam} = 0.55$		$\eta_{beam} = 0.65$	
	$E^{TileCal}$ [GeV]	$\sigma^{TileCal}$ [GeV]	$E^{TileCal}$ [GeV]	$\sigma^{TileCal}$ [GeV]	$E^{TileCal}$ [GeV]	$\sigma^{TileCal}$ [GeV]
20	15.03±0.07	2.79±0.07	14.88±0.06	2.74±0.06	14.80±0.07	2.85±0.07
50	40.31±0.08	4.50±0.08	40.6±0.1	4.6±0.1	40.3±0.1	5.0±0.1
100	82.2±0.1	6.9±0.1	82.4±0.1	6.9±0.1	82.6±0.2	7.3±0.2
150	126.7±0.2	9.6±0.2	127.8±0.3	9.3±0.3	128.2±0.3	9.5±0.3
180	152.5±0.2	11.3±0.2	153.5±0.2	11.1±0.2	154.4±0.2	11.5±0.2
200	169.4±0.2	12.2±0.2	170.5±0.3	12.4±0.3	172.5±0.3	12.4±0.3
250	213.1±0.5	13.4±0.6	-	-	-	-
320	269.1±0.6	17.6±0.6	-	-	271.3±0.6	17.9±0.7
350	298.4±0.5	19.3±0.5	300.2±0.5	19.2±0.5	301.3±0.4	18.0±0.4

Table 3: Measured energy response $E^{TileCal}$ and resolution $\sigma^{TileCal}$ for different values of the nominal beam energy and η_{beam} . Only statistical uncertainties are reported.

E_{nom} [GeV]	$\eta_{beam} = 0.20$		$\eta_{beam} = 0.25$		$\eta_{beam} = 0.35$	
	$R^{E^{Comb}}$	$R^{\sigma^{Comb}}$	$R^{E^{Comb}}$	$R^{\sigma^{Comb}}$	$R^{E^{Comb}}$	$R^{\sigma^{Comb}}$
20	0.65±0.01	0.268±0.002	0.66±0.01	0.247±0.002	0.65±0.01	0.248±0.002
50	0.69±0.01	0.199±0.002	0.71±0.01	0.173±0.002	0.70±0.01	0.171±0.002
100	-	-	0.74±0.01	0.132±0.001	0.73±0.01	0.133±0.001
150	0.78±0.01	0.142±0.001	0.77±0.01	0.122±0.001	0.77±0.01	0.125±0.001
180	0.79±0.01	0.137±0.001	0.78±0.01	0.114±0.001	0.78±0.01	0.121±0.001
200	0.79±0.01	0.133±0.001	0.78±0.01	0.114±0.001	0.78±0.01	0.116±0.001
250	0.78±0.01	0.128±0.001	0.77±0.01	0.112±0.001	-	-
320	0.77±0.01	0.131±0.002	0.78±0.01	0.106±0.001	0.77±0.01	0.109±0.002
350	0.78±0.01	0.126±0.001	0.78±0.01	0.103±0.001	0.78±0.01	0.104±0.001
E_{nom} [GeV]	$\eta_{beam} = 0.45$		$\eta_{beam} = 0.55$		$\eta_{beam} = 0.65$	
	$R^{E^{Comb}}$	$R^{\sigma^{Comb}}$	$R^{E^{Comb}}$	$R^{\sigma^{Comb}}$	$R^{E^{Comb}}$	$R^{\sigma^{Comb}}$
20	0.645±0.009	0.246±0.002	0.639±0.009	0.256±0.002	0.617±0.008	0.265±0.003
50	0.70±0.01	0.176±0.001	0.70±0.01	0.181±0.002	0.683±0.009	0.191±0.002
100	0.73±0.01	0.137±0.001	0.72±0.01	0.141±0.001	0.71±0.01	0.151±0.001
150	0.77±0.01	0.127±0.001	0.77±0.01	0.133±0.002	0.76±0.01	0.141±0.002
180	0.77±0.01	0.125±0.001	0.77±0.01	0.128±0.001	0.76±0.01	0.134±0.001
200	0.76±0.01	0.121±0.001	0.77±0.01	0.122±0.001	0.77±0.01	0.132±0.001
250	0.79±0.01	0.109±0.002	-	-	-	-
320	0.78±0.01	0.109±0.002	-	-	0.76±0.01	0.128±0.002
350	0.79±0.01	0.105±0.001	0.79±0.01	0.106±0.001	0.78±0.01	0.115±0.001

Table 4: Energy response ratio $R^{E^{Comb}}$ and fractional resolutions $R^{\sigma^{Comb}}$ measurements obtained for different values of the beam energy and η_{beam} . Statistical and systematic uncertainties are combined in quadrature. The measurement of $R^{\sigma^{Comb}}$ is dominated by the statistical indeterminations.

160 points having the same η_{beam} . The systematic effect on the determination of $R^{E^{Comb}}$ due
to (i) and (ii) was determined for each value of E_{beam} and η_{beam} taking into account the
fraction of energy deposited in the LAr and in TileCal. The systematic uncertainties
162 on the values of $R^{E^{Comb}}$ and $R^{E^{TileCal}}$ due to the source (iii) are uncorrelated and were
estimated to be 1%. The total error on the determination of $R^{E^{Comb}}$ ($R^{E^{TileCal}}$) is $\cong 1.4\%$
164 ($\cong 1.9\%$). The sources (ii) and (iii) dominate in both cases.

The fractional resolutions are defined as $R^{\sigma^{Comb}} = \sigma^{Comb} / E^{Comb}$ and $R^{\sigma^{TileCal}} =$
166 $\sigma^{TileCal} / E^{TileCal}$. The experimental determinations are also reported in Tables 4 and
5. The values of $R^{\sigma^{Comb}}$ ($R^{\sigma^{TileCal}}$) are $\cong 26\%$ ($\cong 19\%$) at 20 GeV and $\cong 12\%$ ($\cong 7\%$) at
168 350 GeV. The uncertainties are dominated by statistics and are $\Delta(R^{\sigma^{Comb}})_{tot} \cong 1\%$ and
 $\Delta(R^{\sigma^{TileCal}})_{tot} \cong 2\%$.

170 The quantities $R^{E^{Comb}}$ and $R^{E^{TileCal}}$ are shown in Figures 5 and 6 respectively (open
circles) as a function of E_{beam} for different values of η_{beam} . They are also shown in
172 Figures 7 and 8 as a function of η_{beam} for different E_{beam} values. In general the values of
the energy response ratios are larger for small values of η_{beam} . The maximum variation
174 observed is 6%. The uncertainties in the four figures include statistical and systematic
effects combined in quadrature. Figures 9 and 10 show the fractional resolutions $R^{\sigma^{Comb}}$
176 and $R^{\sigma^{TileCal}}$ as a function of $1/\sqrt{E_{beam}}$ (open circles) for different values of η_{beam} .
The values of E_{beam} are in GeV. The values of $R^{\sigma^{TileCal}}$ are worse than those obtained
178 analyzing TileCal standalone data [17] as a fraction of Sample 2 showers start in the
LAR cryostat placed in front of the hadronic calorimeter.

E_{nom} [GeV]	$\eta_{beam} = 0.20$		$\eta_{beam} = 0.25$		$\eta_{beam} = 0.35$	
	$R^{E^{TileCal}}$	$R^{\sigma^{TileCal}}$	$R^{E^{TileCal}}$	$R^{\sigma^{TileCal}}$	$R^{E^{TileCal}}$	$R^{\sigma^{TileCal}}$
20	0.77±0.02	0.204±0.004	0.76±0.01	0.179±0.003	0.76±0.02	0.184±0.004
50	0.83±0.02	0.140±0.003	0.81±0.02	0.110±0.003	0.81±0.02	0.110±0.003
100	-	-	0.83±0.02	0.083±0.002	0.82±0.02	0.087±0.003
150	0.89±0.02	0.085±0.002	0.85±0.02	0.075±0.001	0.85±0.02	0.075±0.001
180	0.89±0.02	0.086±0.001	0.85±0.02	0.071±0.001	0.86±0.02	0.072±0.001
200	0.89±0.02	0.086±0.001	0.86±0.02	0.074±0.002	0.86±0.02	0.072±0.001
250	0.88±0.02	0.080±0.001	0.86±0.02	0.071±0.001	-	-
320	0.87±0.02	0.085±0.002	0.85±0.02	0.069±0.001	0.85±0.02	0.065±0.002
350	0.88±0.02	0.082±0.001	0.85±0.02	0.066±0.001	0.86±0.02	0.065±0.001
E_{nom} [GeV]	$\eta_{beam} = 0.45$		$\eta_{beam} = 0.55$		$\eta_{beam} = 0.65$	
	$R^{E^{TileCal}}$	$R^{\sigma^{TileCal}}$	$R^{E^{TileCal}}$	$R^{\sigma^{TileCal}}$	$R^{E^{TileCal}}$	$R^{\sigma^{TileCal}}$
20	0.75±0.01	0.184±0.004	0.74±0.01	0.184±0.004	0.74±0.01	0.189±0.004
50	0.81±0.02	0.112±0.002	0.82±0.02	0.110±0.003	0.82±0.02	0.122±0.003
100	0.83±0.02	0.083±0.001	0.83±0.02	0.084±0.002	0.83±0.02	0.087±0.002
150	0.85±0.02	0.075±0.001	0.86±0.02	0.071±0.002	0.86±0.02	0.072±0.002
180	0.85±0.02	0.074±0.001	0.86±0.02	0.072±0.002	0.86±0.02	0.073±0.001
200	0.85±0.02	0.072±0.001	0.86±0.02	0.072±0.002	0.87±0.02	0.071±0.002
250	0.86±0.02	0.062±0.003	-	-	-	-
320	0.85±0.02	0.065±0.002	-	-	0.86±0.02	0.065±0.002
350	0.86±0.02	0.064±0.002	0.86±0.02	0.063±0.002	0.87±0.02	0.059±0.001

Table 5: Energy response ratio $R^{E^{TileCal}}$ and fractional resolutions $R^{\sigma^{TileCal}}$ measurements obtained for different values of the beam energy and η_{beam} . Statistical and systematic uncertainties are combined in quadrature. The measurement of $R^{\sigma^{TileCal}}$ is dominated by the statistical indeterminations.

The experimental results are well-represented by the parameterization

$$\frac{\sigma}{E} = \frac{a}{\sqrt{E_{beam}}} \oplus b. \quad (11)$$

180 The values of a and b obtained by fitting eq. (11) to the experimental data are
182 reported in Table 6. The values of a (b) are $\cong 100\%$ ($\cong 9\%$) for Sample 1 and $\cong 75\%$
184 ($\cong 5\%$) for Sample 2. The resolution deteriorates for $\eta_{beam}=0.2$ and $\eta_{beam} > 0.45$.
The corresponding functions are superimposed to the measurements in Figs. 9 and 10.
Adding the noise term c/E_{beam} in (11), the fits give values of c compatible with 0 in
agreement with the discussion of Section 4.3.

186 6. Comparison with Monte Carlo simulation results

The experimental results were compared to the predictions of the MC simulation
188 program Geant 4⁴[2, 3]. The MC LAr and TileCal energy scale were obtained using
the results of electron simulations (see Section 4.1). The QGSP-Bertini hadronic show-
190 ering model [18] was used in the simulation. This is the model presently being used in
the simulation of the response of the ATLAS detector to p-p events.

192 In the simulation, the detector material and geometry were fully described [4]. The
spatial and angular distributions of the beam were also tuned to reproduce the experi-
194 mental ones. The mean and spread of the incoming pion beam momentum correspond

⁴The version 4.91 of the program has been used.

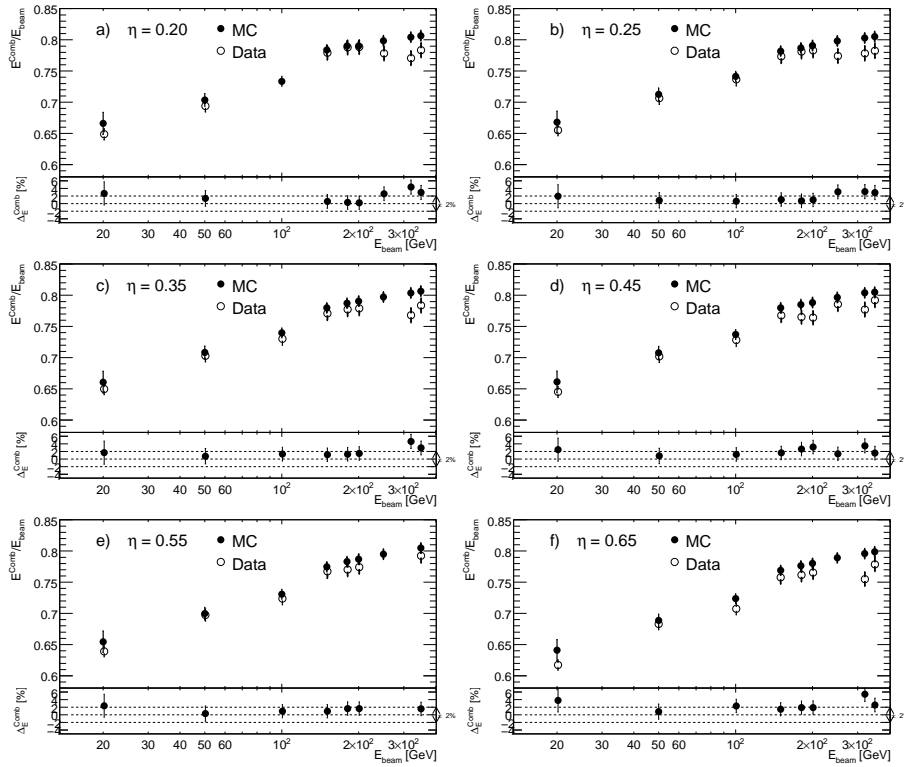


Figure 5: Energy response ratios, $R^{E^{Comb}}$, measured (open circles) and predicted by Monte Carlo simulation (full points) as a function of beam energy for different η_{beam} values: (a) 0.20, (b) 0.25, (c) 0.35, (d) 0.45, (e) 0.55, and (f) 0.65. In the bottom of the histograms are shown the fractional differences Δ_E^{Comb} defined in eq. (12). The dashed horizontal lines indicate the $\pm 2\%$ region. The uncertainty includes statistical and systematic effects combined in quadrature.

to the measured values. The measured electronic noise in the different calorimeter cells and the effects of photo statistic (70 phe/GeV) in the case of the photomultipliers signals, are included in the MC simulation. The simulated events were selected applying the cuts 4-7 of Table 1.

In the case of positive beams at 20, 50 and 100 GeV, the beam pion-proton mixing was included in the MC as was measured using the TRT detector [10]. The values of the proton fractions f_p are reported in Table 7. In the case of the point at 20 GeV the values $f_p = 0.0 \pm 0.2$ was used.

The distributions of E_{raw}^{Comb} and $E_{raw}^{TileCal}$ obtained with simulated data are shown in Figs. 3 and 4 respectively for beam energies 50 GeV (a), 150 GeV (b), 250 GeV (c) and 350 GeV (d) at $\eta=0.35$. As in the case of experimental data, Gauss functions were fit to the data. Figures 5-10 compare the MC results (full points) and the experimental ones (open points). The results of the fit of eq. (11) to the simulated data of Figures 9 and 10 are reported in Table 6. The corresponding functions are superimposed to the data in

Sample 1				
	$R^{\sigma^{Comb}}$ (Experimental data)		$R^{\sigma^{Comb}}$ (Simulated data)	
η_{beam}	a [% · GeV ^{1/2}]	b [%]	a [% · GeV ^{1/2}]	b [%]
0.20	113±1	10.9±0.1	95.5±0.7	10.3±0.1
0.25	103±1	8.8±0.1	87.8±0.6	9.2±0.1
0.35	103±1	9.0±0.1	89.2±0.6	9.7±0.1
0.45	104±1	9.3±0.1	88.9±0.5	9.5±0.1
0.55	110±1	9.4±0.1	92.1±0.6	10.0±0.1
0.65	112±1	10.4±0.1	94.5±0.6	10.0±0.1
Sample 2				
	$R^{\sigma^{TheCal}}$ (Experimental data)		$R^{\sigma^{TheCal}}$ (Simulated data)	
η_{beam}	a [% · GeV ^{1/2}]	b [%]	a [% · GeV ^{1/2}]	b [%]
0.20	82±2	6.3±0.1	76.5±1.3	6.3±0.1
0.25	68±1	5.4±0.1	69.8±1.0	5.8±0.1
0.35	74±2	4.9±0.1	66.7±2.1	5.6±0.1
0.45	72±1	4.9±0.1	68.0±1.0	4.9±0.1
0.55	72±2	4.8±0.2	70.0±1.0	4.8±0.1
0.65	80±2	4.1±0.2	74.1±1.0	4.4±0.1

Table 6: Values of the parameters a and b obtained fitting the resolution parameterization (11) to the experimental and simulated Sample 1 and Sample 2 data. The values of E_{beam} in the square roots are in GeV.

E_{nom} [GeV]	f_p
20	-0.15±0.32
50	0.45±0.12
100	0.61±0.06

Table 7: Fractions of proton particles in positive beams.

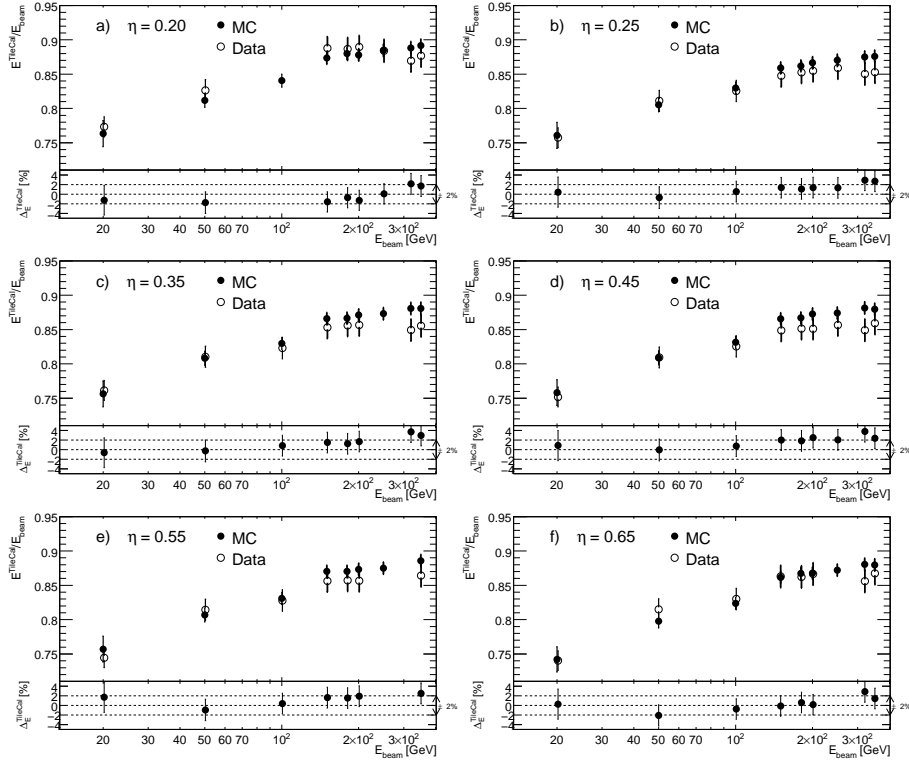


Figure 6: Energy response ratios, $R^{E^{TileCal}}$, measured (open circles) and predicted by Monte Carlo simulation (full points) as a function of beam energy for different η_{beam} values: (a) 0.20, (b) 0.25, (c) 0.35, (d) 0.45, (e) 0.55, and (f) 0.65. In the bottom of the histograms are shown the fractional differences $\Delta_E^{TileCal}$ defined in eq. (13). The dashed horizontal lines indicate the $\pm 2\%$ region. The uncertainty includes statistical and systematic effects combined in quadrature.

the figures. In the case of Sample 1 (Sample 2) values of a obtained using simulated data are about 15% (7%) smaller than those obtained analyzing experimental data. For the two samples the values of b obtained by fitting the experimental and simulated data are closer. The comparison between the data and the simulation can be quantified using the quantities

$$\Delta_E^{Comb} = (E^{Comb})_{MC}/E^{Comb} - 1 \quad (12)$$

$$\Delta_\sigma^{Comb} = (\sigma^{Comb})_{MC}/\sigma^{Comb} - 1$$

and

$$\Delta_E^{TileCal} = (E^{TileCal})_{MC}/E^{TileCal} - 1 \quad (13)$$

$$\Delta_\sigma^{TileCal} = (\sigma^{TileCal})_{MC}/\sigma^{TileCal} - 1$$

The values in percent are reported in Tables 8 and 9 and Figures 5-10. The uncertainties on Δ_E^{Comb} and $\Delta_E^{TileCal}$ are dominated by systematic. The contributions of the

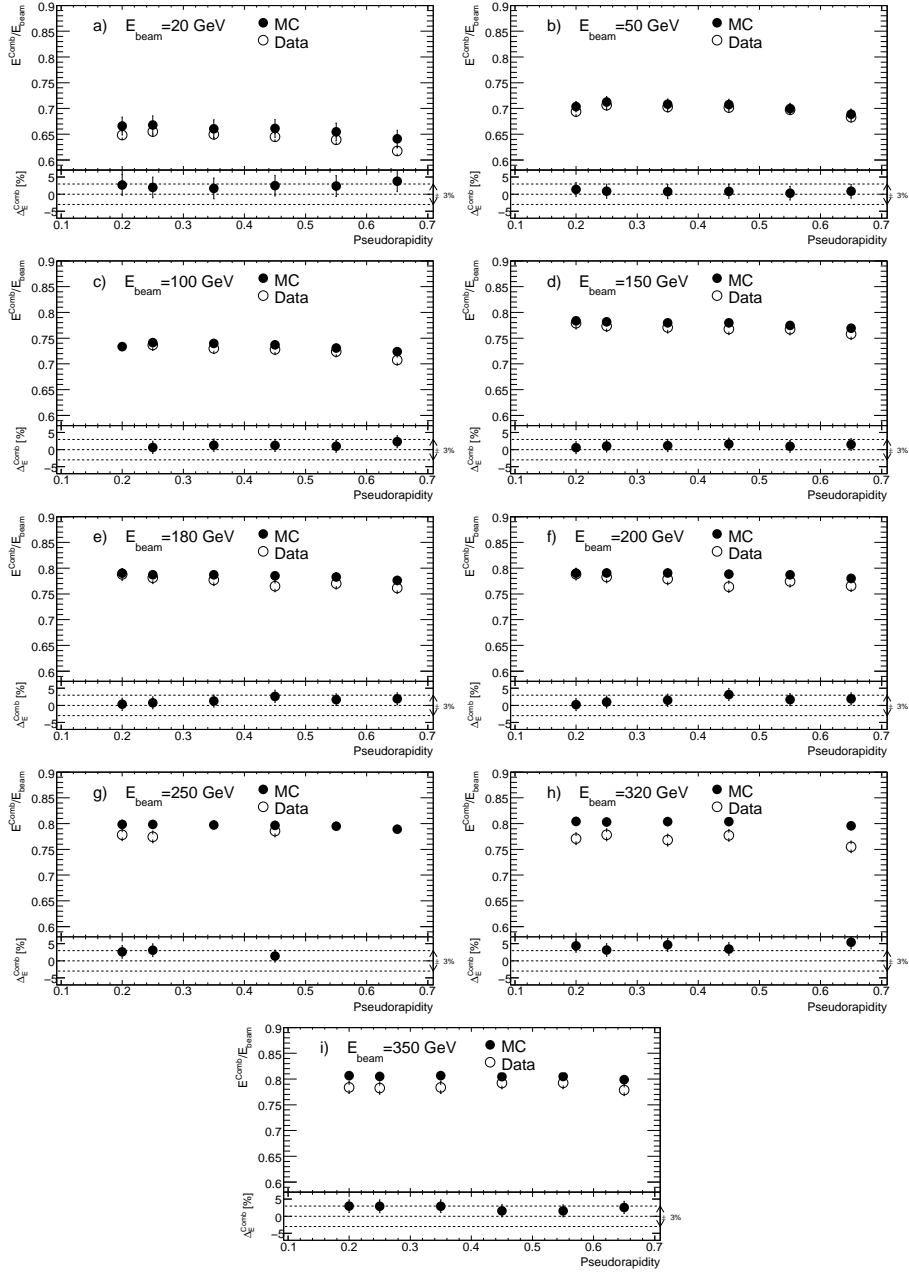


Figure 7: Energy response ratios, $R^{E^{Comb}}$, measured (open circles) and predicted by Monte Carlo simulation (full points) as a function of η_{beam} for different beam energy values: (a) 20 GeV, (b) 50 GeV, (c) 100 GeV, (d) 150 GeV, (e) 180 GeV, (f) 200 GeV, (g) 250 GeV, (h) 320 GeV and (i) 350 GeV. In the bottom of the histograms are shown the fractional differences Δ_{E}^{Comb} defined in eq. (12). The dashed horizontal lines indicate the $\pm 3\%$ region. The uncertainty includes statistical and systematic effects combined in quadrature.

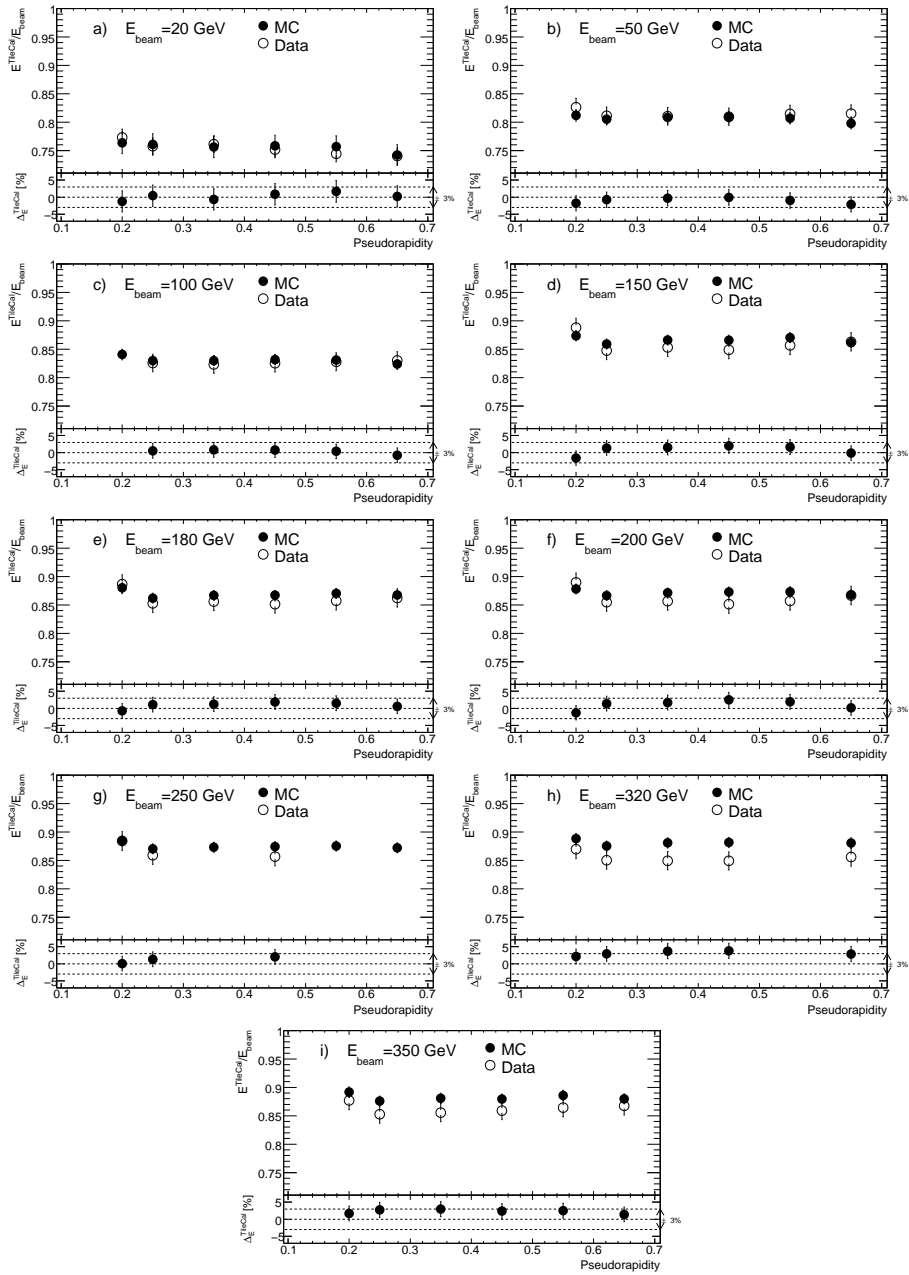


Figure 8: Energy response ratios, $R^{E^{TiteCal}}$, measured (open circles) and predicted by Monte Carlo simulation (full points) as a function of η_{beam} for different beam energy values: (a) 20 GeV, (b) 50 GeV, (c) 100 GeV, (d) 150 GeV, (e) 180 GeV, (f) 200 GeV, (g) 250 GeV, (h) 320 GeV and (i) 350 GeV. In the bottom of the histograms are shown the fractional differences $\Delta_E^{TiteCal}$ defined in eq. (13). The dashed horizontal lines indicate the $\pm 3\%$ region. The uncertainty includes statistical and systematic effects combined in quadrature.

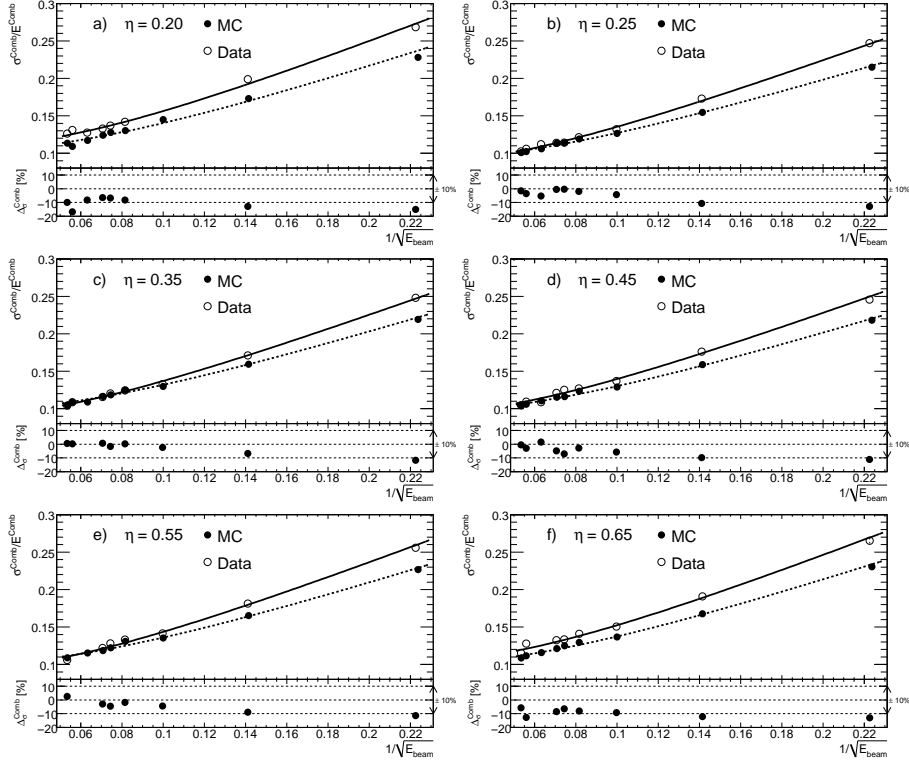


Figure 9: Fractional resolution, $R\sigma^{Comb}$, measured (open circles) and predicted by Monte Carlo simulation (full points) as a function of $1/\sqrt{E_{beam}}$ for different η_{beam} values: (a) 0.20, (b) 0.25, (c) 0.35, (d) 0.45, (e) 0.55, and (f) 0.65. In the bottom of the histograms are shown the fractional differences Δ_{σ}^{Comb} defined in eq. (12). The values of E_{beam} in the square roots are in GeV. The dashed horizontal lines indicate the $\pm 10\%$ region. The uncertainty includes statistical and systematic effects combined in quadrature. The solid (dashed) curves are fits of the function (11) to the data (MC) points.

sources (i)-(iii) are discussed in Section 5.2. In the case of positive beams the effect due to pion-proton mixing, ranging between 2.4% at 20 GeV and 0.4% at 100 GeV, was added in quadrature. The uncertainties on Δ_{σ}^{Comb} and $\Delta_{\sigma}^{TileCal}$ are dominated by statistics (See Section 5.2).

In the case of Sample 1 the response of simulated data is larger and more significant in the case of beam energies equal to 20 GeV and larger than 250 GeV. The maximum difference is 5%. The values of $\Delta_{\sigma}^{TileCal}$ are compatible with 0 for all the energies. The values of Δ_{σ}^{Comb} are always negative showing that the simulated distributions are narrower. Values $\cong -12\%$ have been obtained for beam energies below 100 GeV and, independently of the energy, for $\eta=0.20$ and 0.65. Unstable values of $\Delta_{\sigma}^{TileCal}$ have been obtained. For $E_{nom}=20$ GeV one has $\Delta_{\sigma}^{TileCal} \cong -10\%$. They become positive and equal to few percent for energies larger than 100 GeV and $\eta=0.25$ and 0.35.

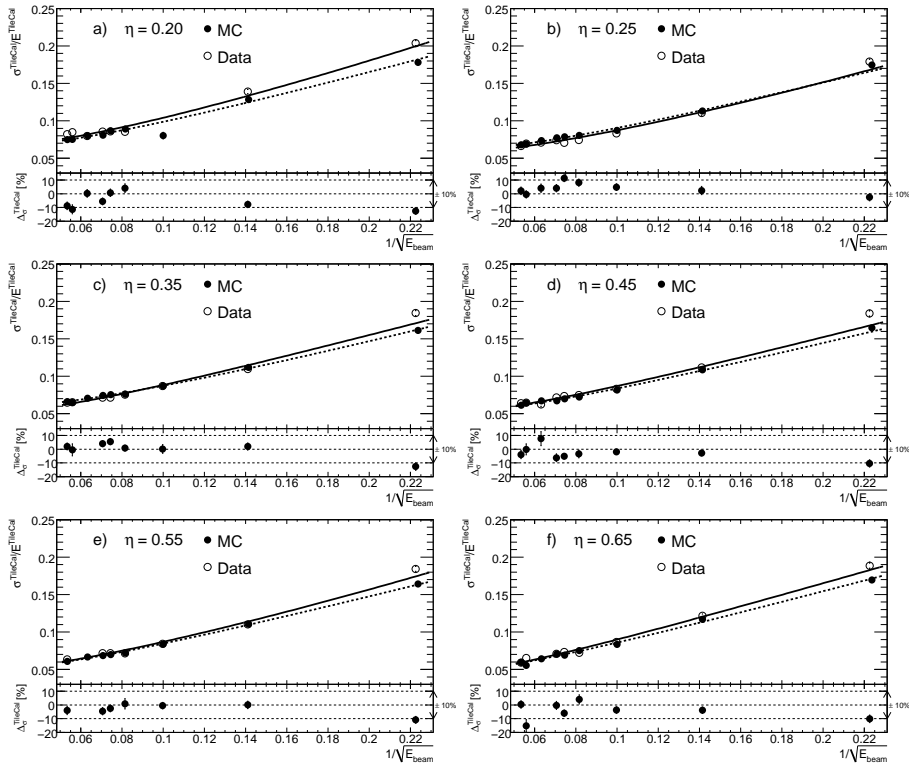


Figure 10: Fractional resolution, $R\sigma^{TileCal}$, measured (open circles) and predicted by Monte Carlo simulation (full points) as a function of $1/\sqrt{E_{beam}}$ for different η_{beam} values: (a) 0.20, (b) 0.25, (c) 0.35, (d) 0.45, (e) 0.55, and (f) 0.65. In the bottom of the histograms are shown the fractional differences $\Delta_{\sigma}^{TileCal}$ defined in eq. (13). The values of E_{beam} in the square roots are in GeV. The dashed horizontal lines indicate the $\pm 10\%$ region. The uncertainty includes statistical and systematic effects combined in quadrature. The solid (dashed) curves are fits of the function (11) to the data (MC) points.

7. Conclusion

218 The characterization of the response of the ATLAS calorimeters to hadrons is im-
 220 portant as many strategies for establishing the jet-energy scale rely on the Monte Carlo
 simulation of the calorimeters. Test beam data are very important to constrain, test and
 validate the simulation models.

222 In this paper, a detailed analysis of the response of the electromagnetic and hadronic
 central calorimeter to hadron beams is presented. Data with energies between 20 and
 224 350 GeV and an incident angle corresponding to pseudo-rapidities between 0.2 and
 0.65 were analyzed. The reconstructed energies were obtained without any correction
 226 for dead material and non-compensation of the calorimeters. The response of TileCal
 to hadrons that start showering after the LAr calorimeter has also been determined.
 228 Considering the statistical and systematic uncertainties, the ratio between the recon-
 structed hadron energy and the beam energy $R^{E^{Comb}}$ ($R^{E^{TileCal}}$) has been determined

E_{nom} [GeV]	$\eta_{beam}=0.20$	$\eta_{beam}=0.25$	$\eta_{beam}=0.35$	$\eta_{beam}=0.45$	$\eta_{beam}=0.55$	$\eta_{beam}=0.65$
	$\Delta_E^{Comb} = [(E^{Comb})_{MC}/E^{Comb} - 1]\%$					
20	3±3	2±3	2±3	3±3	2±3	4±3
50	1±2	1±2	1±2	1±2	0±2	1±2
100	-	1±2	1±2	1±2	1±2	2±2
150	1±2	1±2	1±2	2±2	1±2	2±2
180	0±2	1±2	1±2	3±2	2±2	2±2
200	0±2	1±2	2±2	3±2	2±2	2±2
250	3±2	3±2	-	1±2	-	-
320	4±2	3±2	5±2	4±2	-	5±2
350	3±2	3±2	3±2	2±2	2±2	3±2
	$\Delta_\sigma^{Comb} = [(\sigma^{Comb})_{MC}/\sigma^{Comb} - 1]\%$					
20	-15±1	-13±1	-12±1	-11±1	-11±1	-13±1
50	-13±1	-11±1	-7±1	-10±1	-9±1	-12±1
100	-	-4±1	-2±1	-6±1	-4±1	-9±1
150	-8±1	-2±1	0±1	-3±1	-2±2	-8±1
180	-7±1	-0±1	-2±1	-7±1	-5±1	-7±1
200	-7±1	-1±1	1±1	-5±1	-3±1	-9±1
250	-8±1	-5±1	-	2±2	-	-
320	-17±1	-4±1	0±2	-3±2	-	-13±2
350	-10±1	-2±1	1±1	-1±1	3±1	-6±1

Table 8: Relative difference of response (top) and resolution (bottom) between data and simulated results in the case Sample 1 events, for different values of the beam energies and pseudo-rapidity. The uncertainties were obtained combining in quadrature the statistical and the systematic effects as discussed in the text.

E_{nom} [GeV]	$\eta_{beam}=0.20$	$\eta_{beam}=0.25$	$\eta_{beam}=0.35$	$\eta_{beam}=0.45$	$\eta_{beam}=0.55$	$\eta_{beam}=0.65$
	$\Delta_E^{TileCal} = [(E^{TileCal})_{MC}/E^{TileCal} - 1]\%$					
20	-1±3	0±3	-1±3	1±3	2±3	0±3
50	-2±2	-1±2	-0±2	0±2	-1±2	-2±2
100	-	1±2	1±2	1±2	0±2	-1±2
150	-2±2	1±2	2±2	2±2	2±2	-0±2
180	-1±2	1±2	1±2	2±2	2±2	1±2
200	-1±2	1±2	2±2	2±2	2±2	0±2
250	0±2	1±2	-	2±2	-	-
320	2±2	3±2	4±2	4±2	-	3±2
350	2±2	3±2	3±2	2±2	3±2	1±2
	$\Delta_\sigma^{TileCal} = [(\sigma^{TileCal})_{MC}/\sigma^{TileCal} - 1]\%$					
20	-13±2	-3±3	-13±3	-10±3	-11±2	-10±3
50	-8±2	2±3	2±3	-3±2	0±3	-4±2
100	-	5±2	0±3	-2±2	-0±2	-4±2
150	4±3	8±3	1±2	-3±3	1±4	4±3
180	1±3	11±3	6±2	-5±2	-3±3	-6±2
200	-6±3	4±3	4±2	-6±3	-5±3	-0±3
250	0±3	4±3	-	8±5	-	-
320	-11±3	-0±3	-0±4	-0±4	-	-15±5
350	-9±3	2±3	2±3	-4±3	-4±3	0±3

Table 9: Relative difference of response (top) and resolution (bottom) between data and simulated events in the case of Sample 2 events, for different values of the beam energies and pseudo-rapidity. The uncertainties were obtained combining in quadrature the statistical and the systematic uncertainties as discussed in the text.

230 with a precision equal to $\cong 2.8\%$ ($\cong 2.9\%$) at 20 GeV and $\cong 1.4\%$ ($\cong 1.7\%$) at 350 GeV.
The uncertainty on the fractional resolution $R^{\sigma^{Comb}}$ ($R^{\sigma^{TileCal}}$) is equal to $\cong 1\%$ ($\cong 2\%$)
232 for all the energies. The measurements were compared to simulated results obtained
using Geant 4. The MC simulation is able to reproduce the response to within a few
234 percent. The energy resolution in general is narrower in the simulation than in the data.
The measurements will be compared in the future with those that will be obtained in
236 ATLAS selecting isolated hadronic tracks. The ID measurements would provide the
particle momentum.

238 Acknowledgments

A very important ingredient of the 2004 ATLAS CTB has been the mechanics of
240 the two calorimeters support and movement. We would like to acknowledge Danilo
Giugni, Simone Coelli and Giampiero Braga from INFN Milano for the design, overview
242 of the production and testing of the LAr calorimeter support table. We wish to thank
Claude Ferrari, Pierre Gimenez, Yves Bonnet, Denis Gacon and Alain Pinget of CERN
244 EN/MEF group for the continuous mechanical support provided in the CERN SPS
North Area during the installation of the setup and the data taking. This work was sup-
246 ported in part by the European Community, through the ARTEMIS Research Training
Network (Contract number MRTN-CT-2006-035657) and by GRICES and FCT, Por-
248 tugal

References

- 250 [1] S. Gadomski et al. Deployment and use of the ATLAS DAQ in the Combined
Test Beam. ATL-DAQ-CONF-2005-019, ATL-COM-DAQ-2005-014, 2005.
- 252 [2] S. Agostinelli et al. *Nucl. Instrum. and Meth.*, A506:250 – 303, 2003.
- [3] J. Allison et al. Geant4 developments and applications. *IEEE Transactions on*
254 *Nuclear Science*, 53:270–278, 2006.
- [4] D. Costanzo et al. ATLAS detector simulation: status and outlook.
256 ATL-SOFT-PUB-2005-004, CERN-ATL-SOFT-PUB-2005-004,
ATL-COM-SOFT-2005-008, 2005.
- 258 [5] E. Abat et al. *Nucl. Instrum. and Meth.*, A607(2):372 – 386, 2009.
- [6] B. Chauchaix, I. Efthymiopoulos, and A. Fabich. H8 handbook.
260 (http://nahandbook.web.cern.ch/nahandbook/default/h8/1_General.htm).
- [7] J. Spanggaard. Delay Wire Chambers - A Users Guide. (SL-Note-98-023-BI),
262 Mar 1998.
- [8] B. Girolamo et al. Beamline instrumentation in the 2004 combined ATLAS
264 testbeam. ATLAS-TECH-PUB-2005-001, 2005.

- 266 [9] ATLAS Collaboration. Inner detector Technical Design Report. Technical
Report 1997, CERN, Geneva, Switzerland, CERN/LHCC/97-16, Volume II.
- 268 [10] T. Carli et al. Response and Shower Topology of Pions with Momenta from 2 to
270 180 GeV Measured with the ATLAS Barrel Calorimeter at the CERN Test-beam
and Comparison to Monte Carlo Simulations. ATL-COM-CAL-2009-004, May
2009.
- 272 [11] ATLAS/Liquid Argon Calorimeter Collaboration. Liquid Argon Calorimeter
Technical Design Report. CERN/LHCC 96-41.
- [12] B. Aubert et al. *Nucl. Instrum. and Meth.*, A558(2):388 – 418, 2006.
- 274 [13] ATLAS collaboration. Tile Calorimeter Technical Design report. CERN,
Geneva, Switzerland, CERN/LHCC/96-42.
- 276 [14] ATLAS Collaboration. Muon spectrometer Technical Design Report. Technical
report, CERN, Geneva, Switzerland, CERN/LHCC/97-022.
- 278 [15] M. Aleksa et al. ATLAS Combined Testbeam: Computation and Validation of
the Electronic Calibration Constants for the Electromagnetic Calorimeter.
280 ATL-LARG-PUB-2006-003, 2006.
- [16] M. Aharrouche et al. *Nucl. Instrum. and Meth.*, A614:400–432, 2010.
- 282 [17] P. Adragna et al. *Nucl. Instrum. Meth.*, A606:362–394, 2009.
- [18] H. W. Bertini and P. Guthrie. *Nucl. Instr. and Meth.*, A169:670, 1971.